

# Shear-driven solidification and nonlinear elasticity in epithelial tissues

Junxiang Huang,<sup>1</sup> James O. Cochran,<sup>2</sup> Suzanne M. Fielding,<sup>2</sup> M. Cristina Marchetti,<sup>3</sup> and Dapeng Bi<sup>1</sup>

<sup>1</sup>*Department of Physics, Northeastern University, MA, USA*

<sup>2</sup>*Department of Physics, Durham University, Science Laboratories, South Road, Durham DH1 3LE, UK*

<sup>3</sup>*Department of Physics, University of California, Santa Barbara, CA, USA*

Biological processes, from morphogenesis to tumor invasion, spontaneously generate shear stresses inside living tissue. The mechanisms that govern the transmission of mechanical forces in epithelia and the collective response of the tissue to bulk shear deformations remain, however, poorly understood. Using a minimal cell-based computational model, we investigate the constitutive relation of confluent tissues under simple shear deformation. We show that an undeformed fluid-like tissue acquires finite rigidity above a critical applied strain. This is akin to the shear-driven rigidity observed in other soft matter systems. Interestingly, shear-driven rigidity in tissue is a first-order transition and can be understood as arising from the second order critical point that governs the liquid-solid transition of the undeformed system. We further show that a solid-like tissue responds linearly only to infinitesimally small strains and rapidly switches to a nonlinear response, with substantial stress stiffening. Finally, we propose a mean-field formulation for cells under shear that offers a simple physical explanation of shear-driven rigidity and nonlinear response in a tissue.

Monolayers of tightly connected cells provide essential physical barriers and filters to all organs *in vivo*. The tight connections between cells, with no intervening gaps, allow the tissue to resist external deformation and withstand stress, while maintaining its integrity. At the single cell level, researchers have used a broad repertoire of experimental techniques [1–6] to reveal a rich plethora of mechanical behaviors, including power-law rheology [7] and stress stiffening [8]. At the mesoscopic level, traction force microscopy has allowed the mapping of intercellular forces [9–11], revealing a rough stress landscape, with spatial fluctuations correlated over several cells [12–15].

There is increasing consensus that mechanical deformations can directly influence collective cell behavior [16–20] and play a central role in driving developmental processes [21–28], physiology [14, 29–33], and tumor progression [34–36]. Recent experiments [30, 37–39] have shown that epithelial monolayers respond nonlinearly to external mechanical stretch, with observed stress-stiffening and even fracturing. Similar behavior has also been observed in tissues deformed by internal active motile forces [40] and in curved epithelial sheets enclosing an expanding lumen [41]. Importantly, these experimental studies have typically focused on probing the behavior of solid-like tissue, where cells do not spontaneously exchange neighbors. On the other hand, the last decade has seen a surge of evidence demonstrating that living tissue can spontaneously undergo transitions between a solid-like (jammed) state and a fluid-like (unjammed) state. [42–53]. Despite its fundamental importance and direct relevance to biology, the response of a cell collective to mechanical deformation *at the tissue level* remains poorly understood, especially in the vicinity of the tissue solid-fluid transition.

A growing number of theoretical studies has begun to address this gap. Various groups have used vertex-based models [54, 55] to simulate the linear [56, 57] and nonlinear [58] rheology of a tissue under steady shear flow. The effects of active tension fluctuations [58, 59] and cell division [60] have been explored. An earlier study [61] has also showed that the

vertex model can reproduce a nonlinear mechanical response qualitatively similar to that observed experimentally [37]. Despite this growing body of work, to date there is no systematic study of the mechanical response of an amorphous epithelial tissue near the solid-fluid transition. Still missing is also a quantitative analysis of the nonlinear response to large deformations, which is highly relevant under physiological conditions [21, 30].

In this paper we use a minimal hybrid cell-vertex model to investigate the tissue linear and nonlinear response to externally imposed simple shear deformations. We show that a tissue which is fluid-like when undeformed acquires rigidity above a threshold value of the applied strain. This is akin to the shear-driven rigidity of fiber networks and shear jamming in granular matter [62]. Interestingly, the onset of shear-driven rigidity in the liquid state is a first-order transition characterized by a discontinuous jump in the tissue shear modulus, where the size of the jump depends on the distance to the second order liquid-solid critical point of the undeformed system. We find that nonlinear elasticity becomes increasingly dominant closer to the critical point. At the critical point, the mechanical response is completely nonlinear. Such critical nonlinearity has also been identified in recent work on a vertex models of regular polygons, where it was shown to arise from purely geometric constraints. [63]. We also show that a solid tissue undergoes stiffening when the applied stress exceeds a critical threshold. Finally, we present a mean-field formulation that fully accounts for the emergence of shear-induced rigidity in the liquid state and predicts exactly the nonlinear response and stress-stiffening exponents observed in the simulations.

*Model*— We model a 2D cell layer using the Voronoi-based implementation [64, 65] of the vertex model [51, 55, 66–69]. Here, the cell centers  $\{\mathbf{r}_i\}$  are the degrees of freedom and their Voronoi tessellation determine the cellular structure [64]. The mechanics of the cell layer is governed by the energy function [70]  $E = \sum_{i=1}^N [K_A(A_i - A_0)^2 + K_P(P_i - P_0)^2]$ . The first term, quadratic

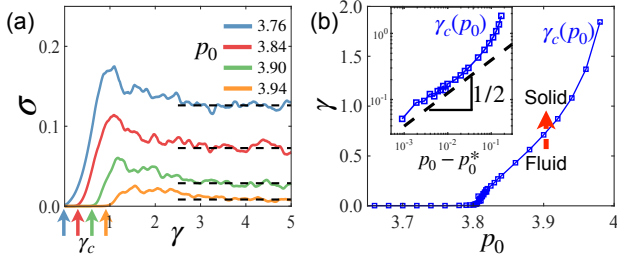


Figure 1. **Tissue mechanical response under quasistatic simple shear.** (a) Stress-strain trace at different  $p_0$  and  $\kappa_A = 0$ . For an initially fluid-like tissue, strain induces rigidity above a critical threshold  $\gamma_c$ . For each value of  $p_0$ ,  $\gamma_c$  is indicated by vertical arrows. (b) The critical strain  $\gamma_c(p_0)$  defines a boundary that separates a fluid-like tissue from a solid-like tissue under strain.

in the cell areas  $\{A_i\}$ , originates from the incompressibility of cell volume, giving rise to a 2D area elasticity constant  $K_A$  and preferred area  $A_0$  [55, 70]. The second term quadratic in the cell perimeters  $\{P_i\}$  arises from the contractility of the cell cortex, with an elastic constant  $K_P$  [55]. Here  $P_0$  is the target cell perimeter [71], representing the interfacial tension set by the competition between the cortical tension and the adhesion between adjacent cells [70]. In this work, we focus on the case where all cells have homogeneous single cell parameters  $K_A, K_P, A_0, P_0$ , while noting that the results are easily generalized to a tissue containing cell-to-cell heterogeneity [66] and are not qualitatively affected by this assumption. We choose  $A_0 = \bar{A}$ , the mean cell area, which also serves as the length unit. The resulting non-dimensionalized energy given by

$$E = \sum_{i=1}^N \kappa_A (a_i - 1)^2 + (p_i - p_0)^2, \quad (1)$$

with  $\kappa_A = K_A \bar{A} / K_P$  the rescaled area elasticity. Here  $p_0 = P_0 / \sqrt{\bar{A}}$  is a crucial model parameter called *target cell shape index*. To study tissue response beyond the linear regime [68], we impose quasistatic simple shear using Lees-Edwards boundary conditions [72]. Starting from a strain-free state ( $\gamma = 0$ ), the strain  $\gamma$  is increased in increments of  $\Delta\gamma = 2 \times 10^{-3}$ , while cell center positions are subject to an affine displacement  $\Delta\mathbf{r}_i = \Delta\gamma y_i \hat{x}$ . Following each strain step, Eq. 1 is relaxed using the FIRE algorithm [73] until all forces  $\mathbf{F}_i \equiv -\partial E / \partial \mathbf{r}_i$  are vanishingly small ( $< 10^{-14}$ ). For all results presented in this work, we used 84 random initial configurations for each parameter choice and  $N = 400$  cells unless otherwise indicated.

*Shear strain drives tissue rigidity* – We characterize the mechanical response by computing the tissue-level shear stress [74–76]  $\sigma = \sigma_{xy} \equiv L^{-2} \sum_{i < j} \mathbf{T}_{ij}^x \mathbf{I}_{ij}^y$ , where  $\mathbf{I}_{ij}$  is the vector of the junction shared by cells  $i, j$  and  $L$  is the simulation box size. At each junction, the line tension is given by  $\mathbf{T}_{ij} = \partial E / \partial \mathbf{I}_{ij} = 2[(p_i - p_0) + (p_j - p_0)]$ .

In Fig. 1(a), we show the stress-strain relation for a range of values of the target cell shape index ( $p_0$ ) and area elasticity  $\kappa_A = 0$ . At small  $\gamma \approx 0$ , the behavior recapitulates the linear-

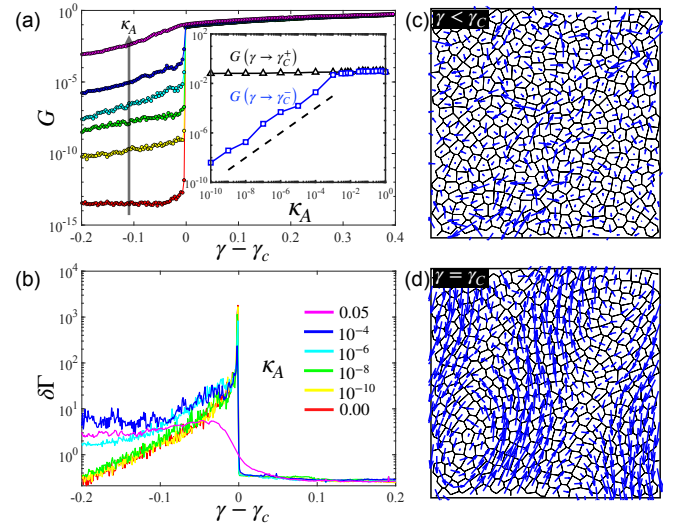


Figure 2. **Strain-driven rigidity transition** (a) The shear modulus  $G$  near the onset of the strain-driven solidification for  $p_0 = 3.84$  and varying values of area elasticity  $\kappa_A = 0, 10^{-10}, 10^{-8}, 10^{-6}, 10^{-4}, 0.05$ . **Inset:** The value of  $G$  immediately below and above the transition show a gap that narrows with increasing  $\kappa_A$ . The dashed line indicates a slope of 1 on the log-log plot. The transition is discontinuous in  $G$  at  $\gamma = \gamma_c$  (b) The Non-affinity parameter  $\Delta\Gamma$  near the onset of the transition for  $p_0 = 3.84$  and varying values of area elasticity  $\kappa_A$ . Maps of non-affine cell displacements before (c) and after (d) the onset of strain stiffening.

response mechanical properties of the vertex model, which has been a focus of previous studies [68, 71, 77]. In short, when the *target shape index*  $p_0$  is below the *critical cell shape index*  $p_0^* = 3.81$  and  $\kappa_A = 0$  the tissue behaves as a rigid solid in the strain-free state, characterized by a non-zero *linear-response* shear modulus  $G_0 \equiv \lim_{\gamma \rightarrow 0} \partial\sigma / \partial\gamma$ . When  $p_0 \geq p_0^*$ ,  $G_0$  becomes vanishingly small, signifying fluidity at the tissue level. This solid-fluid transition at  $\gamma = 0$  driven by cell-cell interactions (encoded by  $p_0$ ) is now well-understood in terms a Maxwell constraint-counting approach [68, 78] and as driven by geometric incompatibility [68, 71, 79–81].

At larger strains ( $\gamma \gtrsim 2$ ), the stress no-longer grows monotonically and the tissue undergoes plastic rearrangements via T1 transitions, resulting in intermittent stick-slip behavior. We define the dynamic yield stress  $\sigma_{\text{yield}}(p_0)$  by averaging the stress values in the plastic regime and plot its value as a function of  $p_0$  in SI-Fig. 6. The yield stress is large in a solid tissue and decreases as  $p_0$  increases, vanishing at  $p_0 \sim 4.03$ . Above this value, the tissue remains fluid-like regardless of the applied shear strain. The vanishing of  $\sigma_{\text{yield}}$  at a value of  $p_0$  larger than  $p_0^*$  suggests that the steady shear flow is decoupled from the shear startup behavior.

The main focus of this work is the stress response beyond the linear regime, but at strains below those yielding plastic flow ( $0 < \gamma < 1$ ), which is also the regime most relevant to experiments [37]. In this regime we show that the linear response ( $\gamma \rightarrow 0$ ) cannot predict what happens at finite strain values. For a tissue that is fluid at  $\gamma = 0$  (i.e., at  $p_0 < p_0^*$ ,

Fig. 1(a)), an applied strain can induce a finite stress when  $\gamma$  reaches a value  $\gamma_C$ . For  $\gamma \geq \gamma_C$ ,  $\sigma$  grows with increasing strain. The stiffening of the liquid upon shear was also reported in recent work on a regular (crystalline) vertex model [56] and in spring-networks [80]. The mean-field analysis below provides a universal explanation for this behavior.

The strain-induced rigidity transition is identified with the line  $\gamma_C(p_0)$  where the instantaneous shear modulus  $G \equiv \partial\sigma/\partial\gamma$  becomes nonzero (Fig. 1(b)). When  $p_0 < p_0^*$ , the undeformed tissue is a solid and  $\gamma_C(p_0) = 0$ . For  $p_0 \in [p_0^*, 4.03]$ , a nonzero value of strain is always required for rigidity and  $\gamma_C(p_0)$  grows monotonically with  $p_0$ . Beyond  $p_0 \gtrsim 4$  it is not possible to obtain a rigid state with *any amount of strain*. This is consistent with a vanishing  $\sigma_{\text{yield}}$  for  $p_0 > 4.03$ .

To understand the nature of strain-induced rigidity, we plot  $G$  near the rigidity onset as a function of  $\gamma - \gamma_C$  (Fig. 2(a)). The nature of the transition depends on the value of the area elasticity,  $\kappa_A$ . At  $\kappa_A = 0$ , the transition from fluid ( $G=0$ ) to solid ( $G>0$ ) is discontinuous. The state for  $\gamma < \gamma_C$  is a marginally rigid state [79, 80] with  $G \approx \kappa_A$  (Fig. 2(a):inset), and the jump discontinuity at  $\gamma_C$  remains finite well above  $\kappa_A > 0$ . At  $\kappa_A \gtrsim 10^{-3}$ , the size of the jump becomes vanishingly small and it is indistinguishable from a continuous increase in  $G$ .

We also examine the nature of fluctuations near the strain-driven rigidity transition using the non-affinity parameter [82–84]  $\delta\Gamma = \frac{1}{N\Delta\gamma^2} \langle (\delta\mathbf{r}_i - \delta\mathbf{r}_i^{\text{affine}})^2 \rangle$ . Here  $\delta\mathbf{r}_i$  is the displacement of cell  $i$  after a strain step and  $\delta\mathbf{r}_i^{\text{affine}} = \Delta\gamma y_i \hat{x}$  is the affine deformation of the cell located at  $\mathbf{r}_i = (x_i, y_i)$ . As shown in Fig. 2(b), at low area elasticity ( $\kappa_A \lesssim 10^{-3}$ ),  $\delta\Gamma$  grows monotonically with strain and exhibits a sharp peak at  $\gamma_C$ , which coincides with the rigidity transition. At higher  $\kappa_A$  values, however, there is no pronounced peak in  $\delta\Gamma$ , indicating a smooth cross-over from the marginal solid to a rigid solid, rather than a discontinuous transition.

*Evolution of cell shapes under shear*— The strain  $\gamma$  is history-dependent and does not uniquely define the state of the tissue due to past plastic events and non-affine deformations. For this reason, we next use the true strain  $\gamma_{\text{true}}$  [85] rather than the applied strain  $\gamma$  to quantify the degree of deformation of the tissue.  $\gamma_{\text{true}}$  is calculated from the instantaneous deformation tensor of the whole tissue (see supplemental materials for details) and therefore captures the degree of *cumulative* strain deformation. The motivation for introducing  $\gamma_{\text{true}}$  is similar to that behind the fabric tensor in granular materials [86] or the recoverable strain in rheology [87]. A plot of  $\sigma$  vs.  $\gamma_{\text{true}}$  shown in Fig. 3(a) displays the stress-strain behavior, albeit without plastic yielding.

Past work on vertex models has shown that the observed cell shape index, given by  $q \equiv \langle p/\sqrt{a} \rangle$ , is an important metric of the tissue state [42, 51], but it is not known how cell shapes evolve with applied shear. In Fig. 3(b), we plot  $q$  against  $\gamma_{\text{true}}$  and observe the relationship

$$q = \begin{cases} p_0, & \gamma_{\text{true}} \leq \gamma_C(p_0) \\ p_0^* + c \gamma_{\text{true}}^2, & \gamma_{\text{true}} > \gamma_C(p_0). \end{cases} \quad (2)$$

This suggests that under shear cell shapes in the fluid stay constant at the *energetically preferred value*  $p_0$  until strain-stiffening, while in the solid  $q$  always starts out at the universal value  $p_0^*$  and grows quadratically with  $\gamma_{\text{true}}$ . A similar functional dependence of the observed cell shape on the cell elongation induced by internally generated active stresses was reported in a recent study of the developing fruit fly [28]. In the next section, we will offer a theoretical derivation of this form.

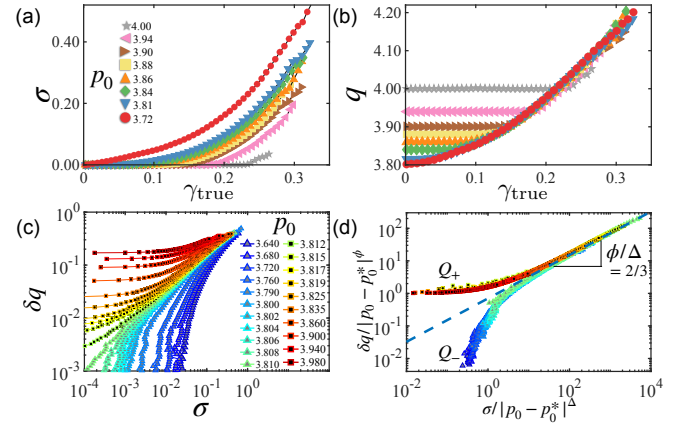


Figure 3. **Cell shapes under shear** (a) A plot of  $\sigma$  as a function of  $\gamma_{\text{true}}$  for different  $p_0$ 's spanning the solid and liquid regimes. (b) The cell shape index  $q$  vs. the true strain  $\gamma_{\text{true}}$  for the same range of  $p_0$  as in (a). (c) A plot of  $\delta q \equiv q - p_0^*$  vs.  $\sigma$  for various values of  $p_0$  as indicated. (d) Replotting of the data from (c) using the universal scaling ansatz (Eq. 3). Here  $\Delta = 3/2$ ,  $\phi = 1$ .

Eq. 2 suggests that the quantity  $\delta q \equiv q - p_0^*$  can be used as a *morphological order parameter*, quantifying the deviation of the measured cell shape from the *critical cell shape*. Moreover, Figs. 3(a,b) suggest that the trio of state variables ( $\sigma, \gamma_{\text{true}}, \delta q$ ) are not independent, and that any two are sufficient to describe the state of the tissue. Therefore, we eliminate  $\gamma_{\text{true}}$  and plot  $\delta q$  as a function  $\sigma$  (Fig. 3(c)) for a large range of  $p_0 \in [3.72, 4]$  below and above  $p_0^*$ . This plot shows typical hallmarks of a critical point, with qualitatively different behavior above and below  $p_0^*$ . We therefore propose an ansatz for universal scaling

$$\delta q = |p_0 - p_0^*|^\phi Q_\pm \left( \frac{\sigma}{|p_0 - p_0^*|^\Delta} \right), \quad (3)$$

where  $Q_\pm(x)$  are the branches of the universal scaling function for  $p_0 > p_0^*$  and  $p_0 \leq p_0^*$ , respectively, with  $x = \sigma / |p_0 - p_0^*|^\Delta$ . Fig. 3(d) shows that this ansatz provides a nearly perfect collapse of the data, with  $\Delta = 3/2$  and  $\phi = 1$ . For  $p_0 > p_0^*$  the behavior is controlled  $Q_+(x)$ , with  $Q_+(x) \rightarrow \text{constant}$  for  $x \rightarrow 0$ , i.e.,  $\sigma \rightarrow 0$ , implying  $\delta q \propto |p_0 - p_0^*|^\phi$ . On the other hand, when  $p_0 < p_0^*$ , the scaling is controlled by  $Q_-(x)$ . In the limit of  $\delta q \rightarrow 0$  (i.e.  $y = \delta q / |p_0 - p_0^*|^\phi \rightarrow 0$ ), the inverse of  $Q_-$  tends to a constant, hence  $\sigma \propto |p_0 - p_0^*|^\Delta$ . For

$|p_0 - p_0^*| \rightarrow 0$  and  $\sigma \gg 0$ , the two universal branches merge and  $Q_+(x) = Q_-(x) = x^{\phi/\Delta}$ .

*Tissue stiffening and nonlinear elasticity*— Next we focus on the nature of the mechanical rigidity in tissues strained beyond  $\gamma_C$ . In this regime both the stress  $\sigma$  (Fig. 1a) and the shear modulus  $G$  (Fig. 2a) show *nonlinear behavior*. To quantify this, we use  $\sigma$ , instead of  $\gamma$ , as a state variable and plot  $G$  as a function of  $\sigma$  in Fig. 4a for various  $p_0 \in [3.66, 3.81]$ . At small  $\sigma$ ,  $G = G_0$  is independent of  $\sigma$ , corresponding to linear elasticity. At higher stress, nonlinear elasticity dominates and  $G \propto (\sigma/\sigma_c)^b$ , with  $b = 2/3$ , corresponding to a constitutive relation  $\sigma \propto \gamma^{1-b} = \gamma^3$ . The linear and nonlinear regimes are separated by a critical stress threshold  $\sigma_c(p_0) \sim |p_0 - p_0^*|$ . The linear-response modulus  $G_0$  also shows power-law scaling in  $|p_0 - p_0^*|$  [68, 71]. To summarize this behavior, we propose a scaling ansatz to describe the behavior of  $G$  in the vicinity of the critical point  $p_0^*$

$$G = |p_0 - p_0^*|^\phi G \left( \frac{\sigma}{|p_0 - p_0^*|^\Delta} \right). \quad (4)$$

This form provides an excellent collapse of all our data onto

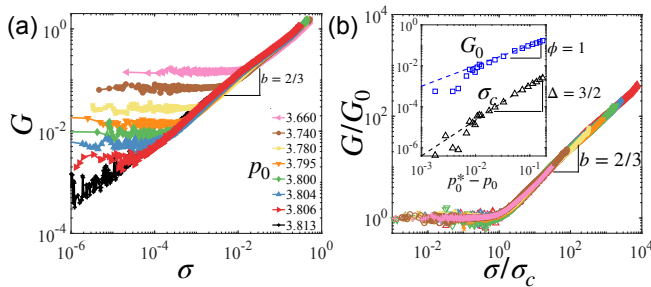


Figure 4. (a) The shear modulus  $G$  vs. stress  $\sigma$  at various  $p_0$ 's and  $\kappa_A = 0$ . (b) Rescaled  $G/G_0$  vs  $\sigma/\sigma_c$  for same set of  $p_0$ 's as in (a).

a single master curve independent of  $p_0$  (Fig. 4b). From the scaling collapse we obtain  $G_0 \propto |p_0 - p_0^*|^\phi$  and  $\sigma_c \propto |p_0 - p_0^*|^\Delta$ , where  $\Delta = 3/2$  and  $\phi = 1$ . Crucially, the stress-stiffening scaling collapse (Eq. 4) is directly related to the cell shape-stress scaling relation (Eq. 3) via  $b = \phi/\Delta$ .

*Mean-field description of a shear-deformed tissue*— To gain a theoretical understanding of the strain-driven rigidity and emergence of nonlinear elasticity, we derive a mean-field theory(MFT) formulation of the vertex model. Neglect cell-cell correlations, we consider the shear deformation of a *single*  $n$ -sided polygonal cell. Under affine deformations, the vertex coordinates of a polygon transform according to  $\mathbf{R}' = \hat{D}\mathbf{R}$ , where  $D$  is the deformation tensor given by  $\hat{D} = \begin{pmatrix} D_{xx} & D_{xy} \\ D_{yx} & D_{yy} \end{pmatrix}$ . We neglect in Eq. 1 the contribution from cell area which is typically small compared to the perimeter term and examine area-preserving affine deformations with  $\det \hat{D} = 1$ . For simple shear  $D_{yx} = 0$  and  $D_{yy} = 1/D_{xx}$ , leaving only  $D_{xx}$  and  $D_{xy}$  as independent components of  $\hat{D}$ .

Considering, for example, a quadrilateral ( $n = 4$ ), the de-

formed perimeter is then given by [88]

$$P = \sqrt{2} \left[ \sqrt{D_{xx}^{-2} + (D_{xx} - D_{xy})^2} + \sqrt{D_{xx}^{-2} + (D_{xx} + D_{xy})^2} \right]. \quad (5)$$

The locus of solutions to Eq. 5 forms *isoperimetric contours* in  $(D_{xx}, D_{xy})$  (Fig. 5(a)). For any  $P > P_{reg} = 4$  [89], there is a degenerate set of quadrilaterals of area 1 that share the common perimeter  $P$ . For any  $P > P_{reg}$ , the maximum value of  $D_{xy}$  along the isoperimetric contour defines the largest simple shear  $D_{xy}^{\max}$  that a cell can sustain by changing its shape, while maintaining its area and perimeter constant, and precisely corresponds to the location of the strain-driven rigidity  $\gamma = \gamma_C$  in the simulations. We obtain  $\gamma_C = D_{xy}^{\max} \propto (p_0 - p_0^*)^{1/2}$ . The exponent 1/2 is in excellent agreement with the  $\gamma_C$  scaling in the vicinity of  $p_0^*$ , shown in Fig. 1:inset.

The isoperimetric contours are centered at  $(D_{xx} = 1, D_{xy} = 0)$  and well approximated by an ellipse for small  $P - P_{reg}$ , we introduce polar coordinates with radius  $M(\theta)$  and polar angle  $\theta$ :  $D_{xx} - 1 = M(\theta) \cos \theta$  and  $D_{xy} = M(\theta) \sin \theta$ . Then Eq. (5) can be expanded [90] to  $O(M^2)$  to give

$$P \approx P_{reg} + \frac{15}{32} P_{reg} \left[ 1 + \frac{3}{5} \cos(2\theta) \right] M(\theta)^2. \quad (6)$$

Using Eq. 6, we rewrite the the vertex model energy(Eq. 1) to obtain a Landau-type energy

$$E_{mf} = \frac{1}{2} t \alpha m(\theta, M)^2 + \frac{1}{4} \beta m(\theta, M)^4, \quad (7)$$

where  $m(\theta, M) = [1 + \frac{3}{5} \cos(2\theta)]^{1/2} M$  is the order parameter,  $\alpha = (60/32)p_0^{*2}$ ,  $\beta = (30/32)p_0^{*2}$  are positive constants, and  $t = (p_0^* - p_0)/p_0^*$  controls the distance to a continuous phase transition in  $m(\theta, M)$ . For  $t > 0$ ,  $E_{mf}$  has a single minimum at  $m^* = 0$  (Fig. 5b), corresponding to the rigid state. When  $t < 0$ , the minimum  $m^*(\theta, M)$  corresponds to the isoperimetrically degenerate liquid state. In the energy landscape these states are connected by a Goldstone mode (Fig. 5c).

The MFT explains the origin of the nonlinear elasticity. For  $t > 0$ , simple shear corresponds to deformations with  $\theta = \pi/2$  and the strain is just given by  $D_{xy} = M$ . The mechanical response can be calculated using Eq. 7

$$\sigma = \partial E_{mf} / \partial M = \alpha t M + \beta M^3 \\ G = \partial^2 E_{mf} / \partial M^2 = \alpha t + 3\beta M^2. \quad (8)$$

For small  $M$  we recover linear elasticity with  $G_0 = \alpha t \propto (p_0^* - p_0)$ . At large  $M$  the response is nonlinear, with  $G \propto \sigma^{2/3}$ . The cross-over stress between the two regimes can be calculated:  $\sigma_c = 2\beta\alpha^{3/2}t^{3/2} \propto (p_0^* - p_0)^{3/2}$ . These predictions are in excellent agreement with simulations results.

*Discussion*— In summary, we have used a Voronoi-based vertex model to study the nonlinear mechanical response of a tissue to shear deformations. A tissue that is fluid-like in the undeformed state, remains fluid up to a critical strain. Using MFT, we show that these fluid states belong to a family

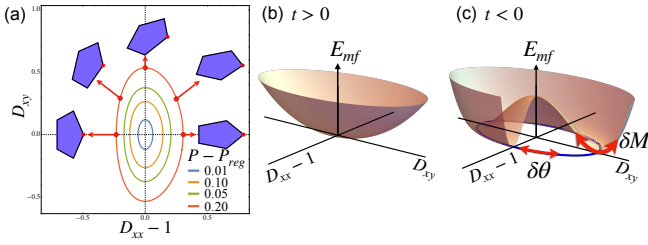


Figure 5. (a) When the perimeter of a polygon is larger than that of its regular counterpart, deformations can lead to a family of isoperimetric shapes defined by the contours shown for a 5-sided polygon at various values of  $P > P_{reg} \approx 3.812$ . (b) The mean-field (MFT) energy landscape as a function of  $(D_{xx} - 1, D_{xy})$  for  $t > 0$  has a unique ground state at  $D_{xx} = 1, D_{xy} = 0$ . (c) The MFT energy landscape as a function of  $(D_{xx} - 1, D_{xy})$  for  $t < 0$  has degenerate ground states which are connected by Goldstone modes in the  $\delta\theta$  direction.

of *isoperimetric degenerate* ground state tissue configurations connected via a Goldstone mode. The isoperimetric degeneracy terminates at a critical strain  $\gamma_C$ . Beyond this point the tissue undergoes strain-stiffening and becomes rigid. This strain-induced rigidity transition is discontinuous, with a jump in the shear modulus. Beyond  $\gamma_C$ , the solid tissues also exhibit strong nonlinear behavior and stress-stiffening, consistent with experimental observations [37].

Here we have focused on shear-startup properties of the tissue, which mimic the behavior in tissue-stretching experiments [30, 37, 38]. Of immediate interest will be to investigate the tissue rheological response to steady-shear at finite strain rate. The results presented here show that the tissue yield stress  $\sigma_{yield}$  and the shear modulus  $G$  do not vanish at the same value of the cell shape index  $p_0$ , suggesting that steady flow and shear startup are governed by different critical points.

## ACKNOWLEDGEMENTS

This work was supported in part by the Northeastern University TIER 1 Grant (J.H. and D.B.), the National Science Foundation (NSF) Grant No. DMR-2046683 (J.H. and D.B.), DMR-2041459 (M.C.M.) and PHY-1748958 (D.B. and M.C.M.). We acknowledge the support of the Northeastern University Discovery Cluster. M.C.M. also thanks Mark Bowick, Michael Moshe and Arthur Hernandez for illuminating discussions.

- [3] Kristina Haase and Andrew E. Pelling, “Investigating cell mechanics with atomic force microscopy,” *Journal of The Royal Society Interface* **12**, 20140970 (2015), <https://royalsocietypublishing.org/doi/pdf/10.1098/rsif.2014.0970>.
- [4] Yifat Brill-Karniely, “Mechanical measurements of cells using afm: 3d or 2d physics?” *Frontiers in Bioengineering and Biotechnology* **8**, 1265 (2020).
- [5] Yuki Fujii, Yuki Ochi, Masahiro Tuchiya, Mihoko Kajita, Yasuyuki Fujita, Yukitaka Ishimoto, and Takaharu Okajima, “Spontaneous spatial correlation of elastic modulus in jammed epithelial monolayers observed by afm,” *Biophysical Journal* **116**, 1152–1158 (2019).
- [6] Friedhelm Serwane, Alessandro Mongera, Payam Rowghanian, David A Kealhofer, Adam A Lucio, Zachary M Hockenberry, and Otger Campas, “In vivo quantification of spatially varying mechanical properties in developing tissues,” *Nature methods* **14**, 181–186 (2017).
- [7] Brenton D. Hoffman, Gladys Massiera, Kathleen M. Van Citters, and John C. Crocker, “The consensus mechanics of cultured mammalian cells,” *Proceedings of the National Academy of Sciences* **103**, 10259–10264 (2006), <https://www.pnas.org/content/103/27/10259.full.pdf>.
- [8] Pablo Fernández, Pramod A Pullarkat, and Albrecht Ott, “A master relation defines the nonlinear viscoelasticity of single fibroblasts,” *Biophysical journal* **90**, 3796–3805 (2006).
- [9] Ulrich S. Schwarz and Jérôme R.D. Soiné, “Traction force microscopy on soft elastic substrates: A guide to recent computational advances,” *Biochimica et Biophysica Acta (BBA) - Molecular Cell Research* **1853**, 3095–3104 (2015), mechanobiology.
- [10] Dhananjay T. Tambe, Ugo Croutelle, Xavier Trepaut, Chan Young Park, Jae Hun Kim, Emil Millet, James P. Butler, and Jeffrey J. Fredberg, “Monolayer stress microscopy: Limitations, artifacts, and accuracy of recovered intercellular stresses,” *PLOS ONE* **8**, 1–12 (2013).
- [11] James P Butler, Iva Marija Tolic-Nørrelykke, Ben Fabry, and Jeffrey J Fredberg, “Traction fields, moments, and strain energy that cells exert on their surroundings,” *American Journal of Physiology-Cell Physiology* **282**, C595–C605 (2002).
- [12] Aaron F. Mertz, Yonglu Che, Shiladitya Banerjee, Jill M. Goldstein, Kathryn A. Rosowski, Stephen F. Revilla, Carien M. Niessen, M. Cristina Marchetti, Eric R. Dufresne, and Valerie Horsley, “Cadherin-based intercellular adhesions organize epithelial cell–matrix traction forces,” *Proceedings of the National Academy of Sciences* **110**, 842–847 (2013), <https://www.pnas.org/content/110/3/842.full.pdf>.
- [13] Aaron F. Mertz, Shiladitya Banerjee, Yonglu Che, Guy K. German, Ye Xu, Callen Hyland, M. Cristina Marchetti, Valerie Horsley, and Eric R. Dufresne, “Scaling of traction forces with the size of cohesive cell colonies,” *Phys. Rev. Lett.* **108**, 198101 (2012).
- [14] Xavier Trepaut, Michael R Wasserman, Thomas E Angelini, Emil Millet, David A Weitz, James P Butler, and Jeffrey J Fredberg, “Physical forces during collective cell migration,” *Nature physics* **5**, 426–430 (2009).
- [15] Jae Hun Kim, Xavier Serra-Picamal, Dhananjay T Tambe, Enhua H Zhou, Chan Young Park, Monirosadat Sadati, Jin-Ah Park, Ramaswamy Krishnan, Bomi Gweon, Emil Millet, *et al.*, “Propulsion and navigation within the advancing monolayer sheet,” *Nature materials* **12**, 856–863 (2013).
- [16] Spiro Getsios, Arthur C Huen, and Kathleen J Green, “Working out the strength and flexibility of desmosomes,” *Nature reviews Molecular cell biology* **5**, 271–281 (2004).

[17] Ning Wang, Jessica D Tytell, and Donald E Ingber, "Mechano-transduction at a distance: mechanically coupling the extracellular matrix with the nucleus," *Nature reviews Molecular cell biology* **10**, 75–82 (2009).

[18] Fabiana Martino, Ana R. Perestrelo, Vladimír Vinarský, Stefania Pagliari, and Giancarlo Forte, "Cellular mechanotransduction: From tension to function," *Frontiers in Physiology* **9**, 824 (2018).

[19] Huimin Zhang and Michel Labouesse, "Signalling through mechanical inputs – a coordinated process," *Journal of Cell Science* **125**, 3039–3049 (2012), <https://journals.biologists.com/jcs/article-pdf/125/13/3039/1922570/jcs-125-13-3039.pdf>.

[20] Tamal Das, Kai Safferling, Sebastian Rausch, Niels Grabe, Heike Boehm, and Joachim P Spatz, "A molecular mechanotransduction pathway regulates collective migration of epithelial cells," *Nature cell biology* **17**, 276–287 (2015).

[21] Peran Hayes and Jérôme Solon, "Drosophila dorsal closure: An orchestra of forces to zip shut the embryo," *Mechanisms of Development* **144**, 2–10 (2017), roles of physical forces in development.

[22] Pedro F. Machado, Julia Duque, Jocelyn Étienne, Alfonso Martínez-Arias, Guy B. Blanchard, and Nicole Gorfinkiel, "Emergent material properties of developing epithelial tissues," *BMC Biology* **13**, 98 (2015).

[23] Deborah J. Andrew and Andrew J. Ewald, "Morphogenesis of epithelial tubes: Insights into tube formation, elongation, and elaboration," *Developmental Biology* **341**, 34 – 55 (2010), special Section: Morphogenesis.

[24] Raphaël Etournay, Marko Popović, Matthias Merkel, Amitabha Nandi, Corinna Blasse, Benoît Aigouy, Holger Brandl, Gene Myers, Guillaume Salbreux, Frank Jülicher, and Suzanne Eaton, "Interplay of cell dynamics and epithelial tension during morphogenesis of the *Drosophila* pupal wing," *eLife* **4**, e07090 (2015).

[25] Boris Guirao, Stéphane U Rigaud, Floris Bosveld, Anaïs Bailles, Jesús López-Gay, Shuji Ishihara, Kaoru Sugimura, François Graner, and Yohanns Bellaïche, "Unified quantitative characterization of epithelial tissue development," *eLife* **4**, e08519 (2015).

[26] Thomas Lecuit, Pierre-François Lenne, and Edwin Munro, "Force generation, transmission, and integration during cell and tissue morphogenesis," *Annual Review of Cell and Developmental Biology* **27**, 157–184 (2011), pMID: 21740231, <https://doi.org/10.1146/annurev-cellbio-100109-104027>.

[27] Robert J Tetley, Michael F Staddon, Davide Heller, Andreas Hoppe, Shiladitya Banerjee, and Yanlan Mao, "Tissue fluidity promotes epithelial wound healing," *Nature Physics* , 1–9 (2019).

[28] Xun Wang, Matthias Merkel, Leo B. Sutter, Gonca Erdemci-Tandogan, M. Lisa Manning, and Karen E. Kasza, "Anisotropy links cell shapes to tissue flow during convergent extension," *Proceedings of the National Academy of Sciences* **117**, 13541–13551 (2020).

[29] Aron B. Fisher, Shu Chien, Abdul I. Barakat, and Robert M. Neren, "Endothelial cellular response to altered shear stress," *American Journal of Physiology-Lung Cellular and Molecular Physiology* **281**, L529–L533 (2001).

[30] Xavier Trepaut, Linhong Deng, Steven S An, Daniel Navajas, Daniel J Tschumperlin, William T Gerthoffer, James P Butler, and Jeffrey J Fredberg, "Universal physical responses to stretch in the living cell," *Nature* **447**, 592–595 (2007).

[31] Jordi Comelles, Soumya SS, Linjie Lu, Emilie Le Maout, S Anitha, Guillaume Salbreux, Frank Jülicher, Mandar M Inamdar, and Daniel Riveline, "Epithelial colonies in vitro elongate through collective effects," *eLife* **10**, e57730 (2021).

[32] Dhananjay T Tambe, C Corey Hardin, Thomas E Angelini, Kavitha Rajendran, Chan Young Park, Xavier Serra-Picamal, Enhua H Zhou, Muhammad H Zaman, James P Butler, David A Weitz, *et al.*, "Collective cell guidance by cooperative intercellular forces," *Nature materials* **10**, 469–475 (2011).

[33] Medhavi Vishwakarma, Jacopo Di Russo, Dimitri Probst, Ulrich S Schwarz, Tamal Das, and Joachim P Spatz, "Mechanical interactions among followers determine the emergence of leaders in migrating epithelial cell collectives," *Nature communications* **9**, 1–12 (2018).

[34] Darci T. Butcher, Tamara Alliston, and Valerie M. Weaver, "A tense situation: forcing tumour progression," *Nature Reviews Cancer* **9**, 108 EP – (2009).

[35] Denis Wirtz, Konstantinos Konstantopoulos, and Peter C Searson, "The physics of cancer: the role of physical interactions and mechanical forces in metastasis," *Nature Reviews Cancer* **11**, 512–522 (2011).

[36] Rakesh K. Jain, John D. Martin, and Triantafyllos Stylianopoulos, "The role of mechanical forces in tumor growth and therapy," *Annual Review of Biomedical Engineering* **16**, 321–346 (2014), pMID: 25014786, <https://doi.org/10.1146/annurev-bioeng-071813-105259>.

[37] Andrew R. Harris, Loic Peter, Julien Bellis, Buzz Baum, Alexandre J. Kabla, and Guillaume T. Charras, "Characterizing the mechanics of cultured cell monolayers," *Proceedings of the National Academy of Sciences* **109**, 16449–16454 (2012), <https://www.pnas.org/content/109/41/16449.full.pdf>.

[38] Nargess Khalilgharibi, Jonathan Fouchard, Nina Asadipour, Ricardo Barrientos, Maria Duda, Alessandra Bonfanti, Amina Yonis, Andrew Harris, Payman Mosaffa, Yasuyuki Fujita, *et al.*, "Stress relaxation in epithelial monolayers is controlled by the actomyosin cortex," *Nature physics* **15**, 839–847 (2019).

[39] Ehsan Sadeghipour, Miguel A Garcia, William James Nelson, and Beth L Pruitt, "Shear-induced damped oscillations in an epithelium depend on actomyosin contraction and e-cadherin cell adhesion," *eLife* **7**, e39640 (2018).

[40] Vivek N Prakash, Matthew S Bull, and Manu Prakash, "Motility-induced fracture reveals a ductile-to-brittle crossover in a simple animal's epithelia," *Nature Physics* **17**, 504–511 (2021).

[41] Ernest Latorre, Sohan Kale, Laura Casares, Manuel Gómez-González, Marina Uroz, Léo Valon, Roshna V Nair, Elena Garreta, Nuria Montserrat, Aránzazu Del Campo, *et al.*, "Active superelasticity in three-dimensional epithelia of controlled shape," *Nature* **563**, 203–208 (2018).

[42] Jin-Ah Park, Jae Hun Kim, Dapeng Bi, Jennifer A. Mitchel, Nader Taheri Qazvini, Kelan Tantisira, Chan Young Park, Maureen McGill, Sae-Hoon Kim, Bomi Gweon, Jacob Notbohm, Robert Steward, Stephanie Burger, Scott H. Randell, Alvin T. Kho, Dhananjay T. Tambe, Corey Hardin, Stephanie A. Shore, Elliott Israel, David A. Weitz, Daniel J. Tschumperlin, Elizabeth P. Henske, Scott T. Weiss, M. Lisa Manning, James P. Butler, Jeffrey M. Drazen, and Jeffrey J. Fredberg, "Unjamming and cell shape in the asthmatic airway epithelium," *Nat Mater* **14**, 1040–1048 (2015).

[43] Simon Garcia, Edouard Hannezo, Jens Elgeti, Jean-François Joanny, Pascal Silberzan, and Nir S. Gov, "Physics of active jamming during collective cellular motion in a monolayer," *Proceedings of the National Academy of Sciences* **112**, 15314–15319 (2015).

[44] Linda Oswald, Steffen Grosser, David M Smith, and Josef A Käs, "Jamming transitions in cancer," *Journal of Physics D: Applied Physics* , (2019).

plied Physics **50**, 483001 (2017).

[45] Colin D Paul, Panagiotis Mistriots, and Konstantinos Konstantopoulos, “Cancer cell motility: lessons from migration in confined spaces,” *Nature Reviews Cancer* **17**, 131–140 (2017).

[46] Chiara Malinverno, Salvatore Corallino, Fabio Giavazzi, Martin Bergert, Qingsen Li, Marco Leoni, Andrea Disanza, Emanuela Frittoli, Amanda Oldani, Emanuele Martini, *et al.*, “Endocytic reawakening of motility in jammed epithelia,” *Nature materials* **16**, 587 (2017).

[47] Lior Atia, Dapeng Bi, Yasha Sharma, Jennifer A Mitchel, Bomi Gweon, Stephan A Koehler, Stephen J DeCamp, Bo Lan, Jae Hun Kim, Rebecca Hirsch, *et al.*, “Geometric constraints during epithelial jamming,” *Nature physics* **14**, 613–620 (2018).

[48] Alessandro Mongera, Payam Rowghanian, Hannah J Gustafson, Elijah Shelton, David A Kealhofer, Emmet K Carn, Friedhelm Serwane, Adam A Lucio, James Giammona, and Otger Campàs, “A fluid-to-solid jamming transition underlies vertebrate body axis elongation,” *Nature* **561**, 401 (2018).

[49] Olga Ilina, Pavlo G. Gritsenko, Simon Syga, Jürgen Lipoldt, Caterina A. M. La Porta, Oleksandr Chepizhko, Steffen Grosser, Manon Vullings, Gert-Jan Bakker, Jörn Starruß, Peter Bult, Stefano Zapperi, Josef A. Käs, Andreas Deutsch, and Peter Friedl, “Cell–cell adhesion and 3d matrix confinement determine jamming transitions in breast cancer invasion,” *Nature Cell Biology* (2020), 10.1038/s41556-020-0552-6.

[50] Robert J. Huebner, Abdul Naseer Malmi-Kakkada, Sena Sarikaya, Shinuo Weng, D. Thirumalai, and John B. Wallingford, “Cadherin clustering controls heterogeneous, asymmetric junction dynamics during vertebrate axis elongation,” *bioRxiv* (2020), 10.1101/2020.02.11.944033.

[51] Jennifer A Mitchel, Amit Das, Michael J O’Sullivan, Ian T Stancil, Stephen J DeCamp, Stephan Koehler, Oscar H Ocaña, James P Butler, Jeffrey J Fredberg, M Angela Nieto, *et al.*, “In primary airway epithelial cells, the unjamming transition is distinct from the epithelial-to-mesenchymal transition,” *Nature communications* **11**, 1–14 (2020).

[52] Nicoletta I. Petridou, Bernat Corominas-Murtra, Carl-Philipp Heisenberg, and Edouard Hannezo, “Rigidity percolation uncovers a structural basis for embryonic tissue phase transitions,” *Cell* **184**, 1914–1928.e19 (2021).

[53] Margherita De Marzio, Ayşe Kılıç, Enrico Maiorino, Jennifer A. Mitchel, Chimwemwe Mwase, Michael J. O’Sullivan, Maureen McGill, Robert Chase, Jeffrey J. Fredberg, Jin-Ah Park, Kimberly Glass, and Scott T. Weiss, “Genomic signatures of the unjamming transition in compressed human bronchial epithelial cells,” *Science Advances* **7**, eabf1088 (2021).

[54] Tatsuzo Nagai and Hisao Honda, “A dynamic cell model for the formation of epithelial tissues,” *Philosophical Magazine B* **81**, 699–719 (2001).

[55] Reza Farhadifar, Jens-Christian Röper, Benoit Aigouy, Suzanne Eaton, and Frank Jülicher, “The influence of cell mechanics, cell-cell interactions, and proliferation on epithelial packing,” *Current Biology* **17**, 2095 – 2104 (2007).

[56] Sijie Tong, Navreeta K. Singh, Rastko Sknepnek, and Andrej Kosmrlj, “Linear viscoelastic properties of the vertex model for epithelial tissues,” (2021), arXiv:2102.11181 [cond-mat.soft].

[57] Marko Popović, Valentin Druelle, Natalie A Dye, Frank Jülicher, and Matthieu Wyart, “Inferring the flow properties of epithelial tissues from their geometry,” *New Journal of Physics* **23**, 033004 (2021).

[58] Charlie Duclut, Joris Pajjmans, Mandar M. Inamdar, Carl D. Modes, and Frank Jülicher, “Nonlinear rheology of cellular networks,” (2021), arXiv:2103.16462 [cond-mat.soft].

[59] Matej Krajnc, Tomer Stern, and Clement Zankoc, “Active instability of cell-cell junctions at the onset of tissue fluidity,” (2021), arXiv:2101.07058 [cond-mat.soft].

[60] Guang-Kui Xu, Yang Liu, and Bo Li, “How do changes at the cell level affect the mechanical properties of epithelial monolayers?” *Soft Matter* **11**, 8782–8788 (2015).

[61] Aziza Merzouki, Orestis Malaspinas, and Bastien Chopard, “The mechanical properties of a cell-based numerical model of epithelium,” *Soft Matter* **12**, 4745–4754 (2016).

[62] Dapeng Bi, Jie Zhang, Bulbul Chakraborty, and Robert P Behringer, “Jamming by shear,” *Nature* **480**, 355–358 (2011).

[63] Arthur Hernandez, Michael F. Staddon, Mark J. Bowick, M. Cristina Marchetti, and Michael Moshe, “Geometric rigidity and anomalous elasticity of cellular tissue vertex model,” in preparation.

[64] Dapeng Bi, Xingbo Yang, M. Cristina Marchetti, and M. Lisa Manning, “Motility-driven glass and jamming transitions in biological tissues,” *Phys. Rev. X* **6**, 021011 (2016).

[65] Bo Li and Sean X. Sun, “Coherent motions in confluent cell monolayer sheets,” *Biophysical Journal*, *Biophysical Journal* **107**, 1532–1541 (2015).

[66] Xinzhi Li, Amit Das, and Dapeng Bi, “Mechanical heterogeneity in tissues promotes rigidity and controls cellular invasion,” *Phys. Rev. Lett.* **123**, 058101 (2019).

[67] Xinzhi Li, Amit Das, and Dapeng Bi, “Biological tissue-inspired tunable photonic fluid,” *Proceedings of the National Academy of Sciences* **115**, 6650–6655 (2018), <https://www.pnas.org/content/115/26/6650.full.pdf>.

[68] Le Yan and Dapeng Bi, “Multicellular rosettes drive fluid-solid transition in epithelial tissues,” *Phys. Rev. X* **9**, 011029 (2019).

[69] Amit Das, Srikanth Sastry, and Dapeng Bi, “Controlled neighbor exchanges drive glassy behavior, intermittency and cell streaming in epithelial tissues,” (2021), arXiv:2003.01042 [cond-mat.soft].

[70] D. B. Staple, R. Farhadifar, J. C. Röper, B. Aigouy, S. Eaton, and F. Jülicher, “Mechanics and remodelling of cell packings in epithelia,” *The European Physical Journal E* **33**, 117–127 (2010).

[71] Dapeng Bi, J. H. Lopez, J. M. Schwarz, and M. Lisa Manning, “A density-independent rigidity transition in biological tissues,” *Nature Physics* **11**, 1074–1079 (2015).

[72] M. P. Allen and D. J. Tildesley, *Computer Simulation of Liquids* (Clarendon Press, New York, NY, USA, 1989).

[73] Erik Bitzek, Pekka Koskinen, Franz Gähler, Michael Moseler, and Peter Gumbusch, “Structural relaxation made simple,” *Phys. Rev. Lett.* **97**, 170201 (2006).

[74] Shuji Ishihara and Kaoru Sugimura, “Bayesian inference of force dynamics during morphogenesis,” *Journal of Theoretical Biology* **313**, 201 – 211 (2012).

[75] Kevin K. Chiou, Lars Hufnagel, and Boris I. Shraiman, “Mechanical stress inference for two dimensional cell arrays,” *PLOS Computational Biology* **8**, 1–9 (2012).

[76] Xingbo Yang, Dapeng Bi, Michael Czajkowski, Matthias Merkel, M. Lisa Manning, and M. Cristina Marchetti, “Correlating cell shape and cellular stress in motile confluent tissues,” *Proceedings of the National Academy of Sciences* (2017).

[77] Daniel M. Sussman and Matthias Merkel, “No unjamming transition in a voronoi model of biological tissue,” *Soft Matter* **14**, 3397–3403 (2018).

[78] Ojan Khatib Damavandi, Varda F. Hagh, Christian D. Santangelo, and M. Lisa Manning, “Energetic rigidity i: A unifying theory of mechanical stability,” (2021), arXiv:2102.11310 [cond-mat.soft].

[79] Michael Moshe, Mark J Bowick, and M Cristina Marchetti, “Geometric frustration and solid-solid transitions in model 2d tissue,” *Physical review letters* **120**, 268105 (2018).

[80] Matthias Merkel, Karsten Baumgarten, Brian P. Tighe, and M. Lisa Manning, “A minimal-length approach unifies rigidity in underconstrained materials,” *Proceedings of the National Academy of Sciences* **116**, 6560–6568 (2019), <https://www.pnas.org/content/116/14/6560.full.pdf>.

[81] Raz Kupferman, Ben Maman, and Michael Moshe, “Continuum mechanics of a cellular tissue model,” *Journal of the Mechanics and Physics of Solids* **143**, 104085 (2020).

[82] Stephen A. Langer and Andrea J. Liu, “Effect of random packing on stress relaxation in foam,” *The Journal of Physical Chemistry B* **101**, 8667–8671 (1997).

[83] B. A. DiDonna and T. C. Lubensky, “Nonaffine correlations in random elastic media,” *Phys. Rev. E* **72**, 066619 (2005).

[84] C. P. Broedersz and F. C. MacKintosh, “Modeling semiflexible polymer networks,” *Rev. Mod. Phys.* **86**, 995–1036 (2014).

[85] Morton E. Gurtin, Eliot Fried, and Lallit Anand, *The Mechanics and Thermodynamics of Continua* (Cambridge University Press, 2010).

[86] J. D. Goddard, “Continuum modeling of granular assemblies,” in *Physics of Dry Granular Media*, edited by H. J. Herrmann, J.-P. Hovi, and S. Luding (Springer Netherlands, Dordrecht, 1998) pp. 1–24.

[87] Piyush K. Singh, Johnny Ching-Wei Lee, Kshitish A. Patankar, and Simon A. Rogers, “Revisiting the basis of transient rheological material functions: Insights from recoverable strain measurements,” *Journal of Rheology* **65**, 129–144 (2021), <https://doi.org/10.1122/8.0000154>.

[88] The perimeter is calculated based on vertex positions  $\mathbf{R}_i$ :  $P = \sum_{i=1}^n |\mathbf{R}_i - \mathbf{R}_{i+1}|$ .

[89] The perimeter of a regular  $n$ -sided polygon with unit area is given by  $P_{reg} = 2\sqrt{n \tan(\frac{\pi}{n})}$ .

[90] Besides the overall factor of  $P_{reg}$ , Eq. 6 holds for all  $n$  except for  $n = 4$ . The quadrilateral ( $n = 4$ ) is a special case, where the perimeter is given by  $P \approx P_{reg} + \frac{1}{16} P_{reg} [9 + 7\cos(2\phi)] M(\phi)^2$ .

[91] Miguel Aubouy, Yi Jiang, James A. Glazier, and Francois Graner, “A texture tensor to quantify deformations,” *Granular Matter* **5**, 67–70 (2003).

[92] Benoît Aigouy, Reza Farhadifar, Douglas B. Staple, Andreas Sagner, Jens-Christian Röper, Frank Jülicher, and Suzanne Eaton, “Cell Flow Reorients the Axis of Planar Polarity in the Wing Epithelium of *Drosophila*,” *Cell* **142**, 773–786 (2010).

[93] F. Graner, B. Dollet, C. Raufaste, and P. Marmottant, “Discrete rearranging disordered patterns, part I: Robust statistical tools in two or three dimensions,” *The European Physical Journal E* **25**, 349–369 (2008).

[94] Matteo Rauzi, Pascale Verant, Thomas Lecuit, and Pierre-François Lenne, “Nature and anisotropy of cortical forces orienting *drosophila* tissue morphogenesis,” *Nature Cell Biology* **10**, 1401 EP – (2008).

[95] F. Bosveld, I. Bonnet, B. Guirao, S. Tlili, Z. Wang, A. Petitallot, R. Marchand, P.-L. Bardet, P. Marcq, F. Graner, and Y. Bellaïche, “Mechanical Control of Morphogenesis by Fat/Dachsous/Four-Jointed Planar Cell Polarity Pathway,” *Science* **336**, 724–727 (2012).

[96] Michael Czajkowski, Dapeng Bi, M. Lisa Manning, and M. Cristina Marchetti, “Hydrodynamics of shape-driven rigidity transitions in motile tissues,” *Soft Matter* **14**, 5628–5642 (2018).

[97] Thomas H Courtney, *Mechanical behavior of materials* (Wiley-Blackwell Press, 2005).

## SUPPLEMENTAL MATERIAL

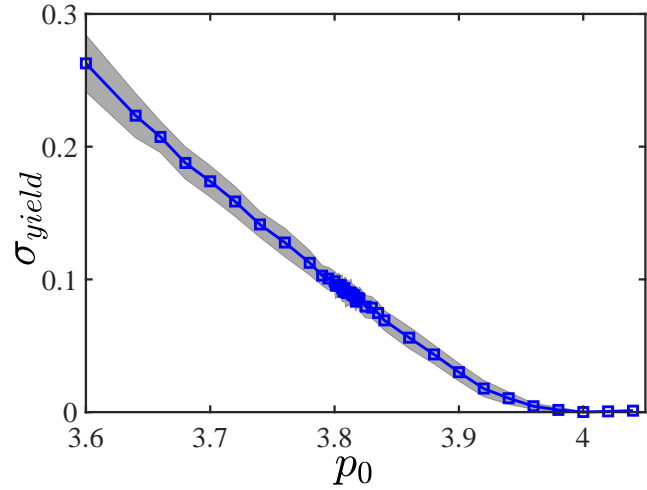


Figure 6. The yield stress  $\sigma_{yield}$  as a function of the target shape index  $p_0$ . The shading in the figure indicates standard variance from different random initial configurations.

## Quantification of the instantaneous tissue deformation using the true strain

Inspired by previous efforts [24, 25, 91–96] on quantifying the degree of deformation in biological tissues, here we propose a method which lifts the restriction in previous approaches that deformation tensor must be symmetric. Our approach can describe not only pure stretching but also general deformation field.

For a single cell, its cell shape tensor is given by [96]

$$\hat{R}_{\alpha\beta} = \frac{1}{A} \int \rho_\alpha \rho_\beta dA. \quad (9)$$

Here  $\rho_\alpha, \rho_\beta$  are cartesian coordinates of points within the cell contour, where  $\alpha, \beta = x, y$ .  $\vec{p}$  is measured from the geometric centroid of the cell.  $A$  is the cell area. The shape tensor  $\hat{R}$  is equivalent to the moment of inertia for the cell and has also been called the texture tensor in previous works [91].

For a cell that is polygonal, the cell shape tensor can be computed by summing over its vertex positions  $\{x_v, y_v\}$ . Its components are given by

$$\begin{aligned}
R_{xx} &= \frac{1}{12A} \sum_{v=1}^z (x_{v-1}^2 + x_{v-1}x_v + x_v^2)(x_{v-1}y_v - x_vy_{v-1}) \\
R_{xy} &= \frac{1}{24A} \sum_{v=1}^z (2x_{v-1}y_{v-1} + x_{v-1}y_v + x_vy_{v-1} + 2x_vy_v)(x_{v-1}y_v - x_vy_{v-1}) \\
R_{yy} &= \frac{1}{12A} \sum_{v=1}^z (y_{v-1}^2 + y_{v-1}y_v + y_v^2)(y_{v-1}x_v - y_vx_{v-1}).
\end{aligned} \tag{10}$$

Where  $z$  is the number of vertices or the coordination number of cell.

Next we consider how a deformation alters the shape tensor. Conventionally, the deformation tensor  $\hat{D}$  is defined as a transformation that maps a coordinate to a deformed one:  $\vec{r}^{(0)} \rightarrow \vec{r}$ . In 2D it is given by,

$$\hat{D} \vec{r}^{(0)} = \begin{pmatrix} D_{xx} & D_{xy} \\ D_{yx} & D_{yy} \end{pmatrix} \begin{pmatrix} x^{(0)} \\ y^{(0)} \end{pmatrix} = \begin{pmatrix} x \\ y \end{pmatrix} = \vec{r}. \tag{11}$$

Application of  $\hat{D}$  on the vertices of a cell results in a transformation of the shape tensor  $\hat{R}^{(0)} \rightarrow \hat{R}$ , which is given by

$$\begin{aligned}
R_{xx} &= D_{xx}^2 R_{xx}^{(0)} + 2D_{xx}D_{xy}R_{xy}^{(0)} + D_{xy}^2 R_{yy}^{(0)} \\
R_{xy} &= D_{xx}D_{yx}R_{xx}^{(0)} + (D_{xx}D_{yy} + D_{xy}D_{yx})R_{xy}^{(0)} + D_{xy}D_{yy}R_{yy}^{(0)} \\
R_{yy} &= D_{yx}^2 R_{xx}^{(0)} + 2D_{yx}D_{yy}R_{xy}^{(0)} + D_{yy}^2 R_{yy}^{(0)}.
\end{aligned} \tag{12}$$

For a tissue that is subject to a affine deformation field  $\hat{D}$  (this is indeed the case away from the strain-stiffening transition), then we can characterize the global shape tensor of the tissue by averaging over all cells  $\{i\}$ :  $\hat{R} = \langle \hat{R}^i \rangle$ . Then the *global shape tensor* and the averaged shape tensor  $\hat{R}$  are also related according to Eq. (12). As the total tissue area is constant, we must have  $\det \hat{D} = 1$ . Then Eq. (12) can be further simplified to

$$\begin{aligned}
\frac{R_{xx}}{\sqrt{\det \hat{R}}} &= D_{xx}^2 + D_{xy}^2 \\
\frac{R_{xy}}{\sqrt{\det \hat{R}}} &= D_{xx}D_{yx} + D_{xy}D_{yy} \\
\frac{R_{yy}}{\sqrt{\det \hat{R}}} &= D_{yx}^2 + D_{yy}^2
\end{aligned} \tag{13}$$

Eq. 13 relates the three independent components of  $\hat{R}$  to the

four independent components of  $\hat{D}$ , which means that components of  $\hat{D}$  are under-constrained. We next set assume the deformation tensor to be symmetric, i.e.  $D_{xy} = D_{yx}$ . This form represents affine pure shear, and is used in previous approaches. Inserting this condition into Eq. (13) leads to

$$\begin{aligned}
D_{xx} &= \frac{R_{xx} + \sqrt{\det \hat{R}}}{\det \hat{R}^{\frac{1}{4}} \sqrt{R_{xx} + R_{yy} + 2\sqrt{\det \hat{R}}}} \\
D_{xy} &= \frac{R_{xy}}{\det \hat{R}^{\frac{1}{4}} \sqrt{R_{xx} + R_{yy} + 2\sqrt{\det \hat{R}}}} \\
D_{yy} &= \frac{R_{yy} + \sqrt{\det \hat{R}}}{\det \hat{R}^{\frac{1}{4}} \sqrt{R_{xx} + R_{yy} + 2\sqrt{\det \hat{R}}}}.
\end{aligned} \tag{14}$$

The resulting  $\hat{D}$  has eigenvalues  $\lambda_{\pm}$  given by

$$\begin{aligned}
\lambda_{\pm} &= \frac{1}{2} \left[ (D_{xx} + D_{yy}) \pm \sqrt{(D_{xx} - D_{yy})^2 + 4D_{xy}^2} \right] \\
&= \frac{\sqrt{R_{xx} + R_{yy} + 2\sqrt{\det \hat{R}}} \pm \sqrt{R_{xx} + R_{yy} - 2\sqrt{\det \hat{R}}}}{2\det \hat{R}^{\frac{1}{4}}}.
\end{aligned} \tag{15}$$

The deformation corresponds to an affine pure shear. We then use the concept of true strain [85, 97] to quantify it, which is defined as

$$\begin{aligned}
\gamma_{\text{true}} &= \log(\lambda_{+}) \\
&= \log \left[ \frac{\sqrt{R_{xx} + R_{yy} + 2\sqrt{\det \hat{R}}} + \sqrt{R_{xx} + R_{yy} - 2\sqrt{\det \hat{R}}}}{2\det \hat{R}^{\frac{1}{4}}} \right].
\end{aligned} \tag{16}$$